

Luminescent *fac*-[ReX(CO)₃(phenyl-pyta)] (X = Cl, Br, I) complexes: Influence of the halide ligand on the electronic properties in solution and in the solid state

Alexandre Poirot, Corinne Vanucci-Bacqué, Béatrice Delavaux-Nicot, Nathalie Saffon-Merceron, Charles-Louis Serpentine, Nadine Leygue, Florence Bedos-Belval, Eric Benoist, Suzanne Fery-Forgues

Synthesis and characterization

Figure S1. Carbon numbering for attribution of ¹ H and ¹³ C NMR chemical shifts	2
Figure S2. ¹ H NMR spectrum of complex 1-Br in CDCl ₃	2
Figure S3. ¹³ C NMR and HSQC spectra of complex 1-Br in CDCl ₃	3
Figure S4. ¹ H NMR spectra of complex 1-I in CDCl ₃ and DMSO-d ₆	4
Figure S5. ¹³ C NMR and HSQC NMR spectra of complex 1-I in DMSO-d ₆	5
Figure S6. Comparison of the ¹ H NMR spectra of complexes 1-Cl , 1-Br and 1-I in CDCl ₃	6

Crystallographic data

Table S1. Selected bond lengths (Å) for complexes 1-Cl , 1-Br and 1-I	6
Table S2. Selected angles (°) for complexes 1-Cl , 1-Br and 1-I	7
Figure S7. Molecular view of the asymmetric unit of complexes 1-Cl , 1-Br and 1-I	8
Figure S8. Crystallographic arrangement of complexes 1-Br and 1-I	8
Figure S9. Crystallographic arrangement of complex 1-Cl	8

Quantum chemistry calculations

Table S3. Composition (%) of the frontier molecular orbitals of complex 1-Cl in CH ₂ Cl ₂	9
Table S4. Main electronic transitions for complex 1-Cl in CH ₂ Cl ₂ calculated using the TD-DFT method	9
Figure S10. Energy levels and isodensity plots of the first frontier molecular orbitals of 1-Cl in CH ₂ Cl ₂	10
Figure S11. Theoretical UV-vis absorption spectrum and main electronic transitions for 1-Cl in CH ₂ Cl ₂	10
Table S5. Composition (%) of the frontier molecular orbitals of complex 1-Br in CH ₂ Cl ₂	11
Table S6. Main electronic transitions for complex 1-Br in CH ₂ Cl ₂ calculated using the TD-DFT method	11
Figure S12. Energy levels and isodensity plots of the first frontier molecular orbitals of 1-Br in CH ₂ Cl ₂	12
Figure S13. Theoretical UV-vis absorption spectrum and main electronic transitions for 1-Br in CH ₂ Cl ₂	12
Table S7. Composition (%) of the frontier molecular orbitals of complex 1-I in CH ₂ Cl ₂	13
Table S8. Main electronic transitions for complex 1-I in CH ₂ Cl ₂ calculated using the TD-DFT method	13
Figure S14. Energy levels and isodensity plots of the first frontier molecular orbitals of 1-I in CH ₂ Cl ₂	14
Figure S15. Theoretical UV-vis absorption spectrum and main electronic transitions for 1-I in CH ₂ Cl ₂	14
Figure S16. Geometry and phenyl-pyta dihedral angle values of complexes 1-Cl , 1-Br and 1-I in the crystal, and in the ground and first triplet excited state	15
Figure S17. Representation of the spin density, geometry and position of unpaired electrons in the triplet state of 1-Cl , 1-Br and 1-I	15

Electrochemistry

Table S9 Selected electrochemical data of complexes 1-Cl , 1-Br and 1-I , determined by OSWV	16
Table S10 Experimental electrochemical data used and calculated values of the energy gaps (<i>E_g</i>)	16
Figure S18. OSWVs: anodic and cathodic scans of complex 1-Br	17
Figure S19. Cyclic voltammograms of 1-Br and of its first oxidation and reduction processes	17
Figure S20. Complex 1-Br : Cyclic voltammograms of the first oxidation process at 1, 5, 10, 50 V/s and of the first reduction process at 1, 5, 10, 20 V/s	17
Figure S21. OSWVs: anodic and cathodic scans of complex 1-I	18
Figure S22. Cyclic voltammograms of 1-I and of its first oxidation and reduction processes	18
Figure S23. Segmented cyclic voltammograms of complex 1-I in oxidation at increasing potential	18
Figure S24. Complex 1-I : Cyclic voltammograms of the first oxidation process at 1, 5, 10 V/s, and of the first reduction process at 10, 20, 50 V/s	18
Figure S25. Cyclic voltammograms of the first oxidation and reduction processes of 1-Cl and 1-Br	19
Figure S26. OSWVs: anodic scans of complexes 1-Br and 1-I	19

Spectroscopy

Figure S27. Emission spectra of the three complexes as microcrystalline pristine powders, after grinding, and after fuming the ground powder with THF during 48h	19
---	----

Fluorescence microscopy

Figure S28. Fluorescence microscopy image of crystals of 1-Cl , 1-Br and 1-I	19
--	----

Synthesis and characterization

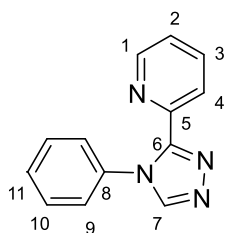


Figure S1. Carbon numbering for attribution of ^1H and ^{13}C NMR chemical shifts.

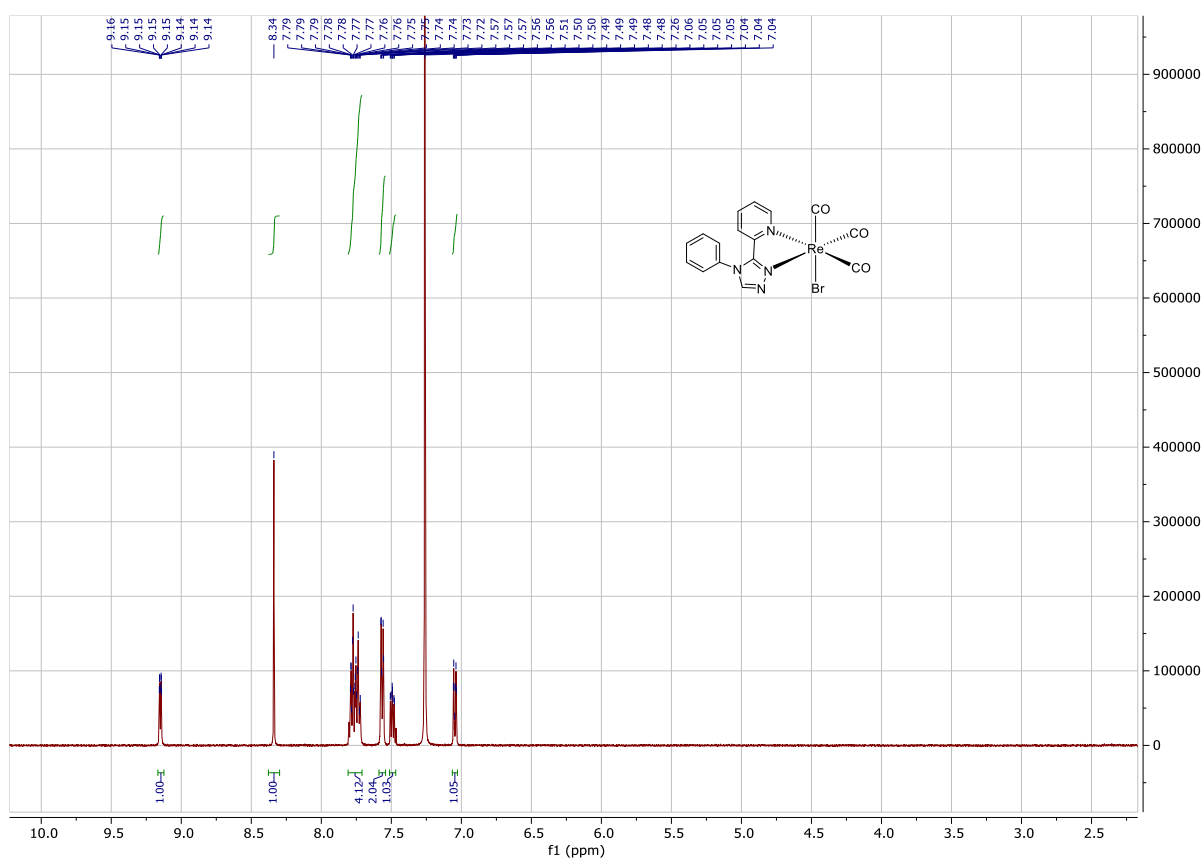


Figure S2. ^1H NMR spectrum of complex **1-Br** in CDCl_3 .

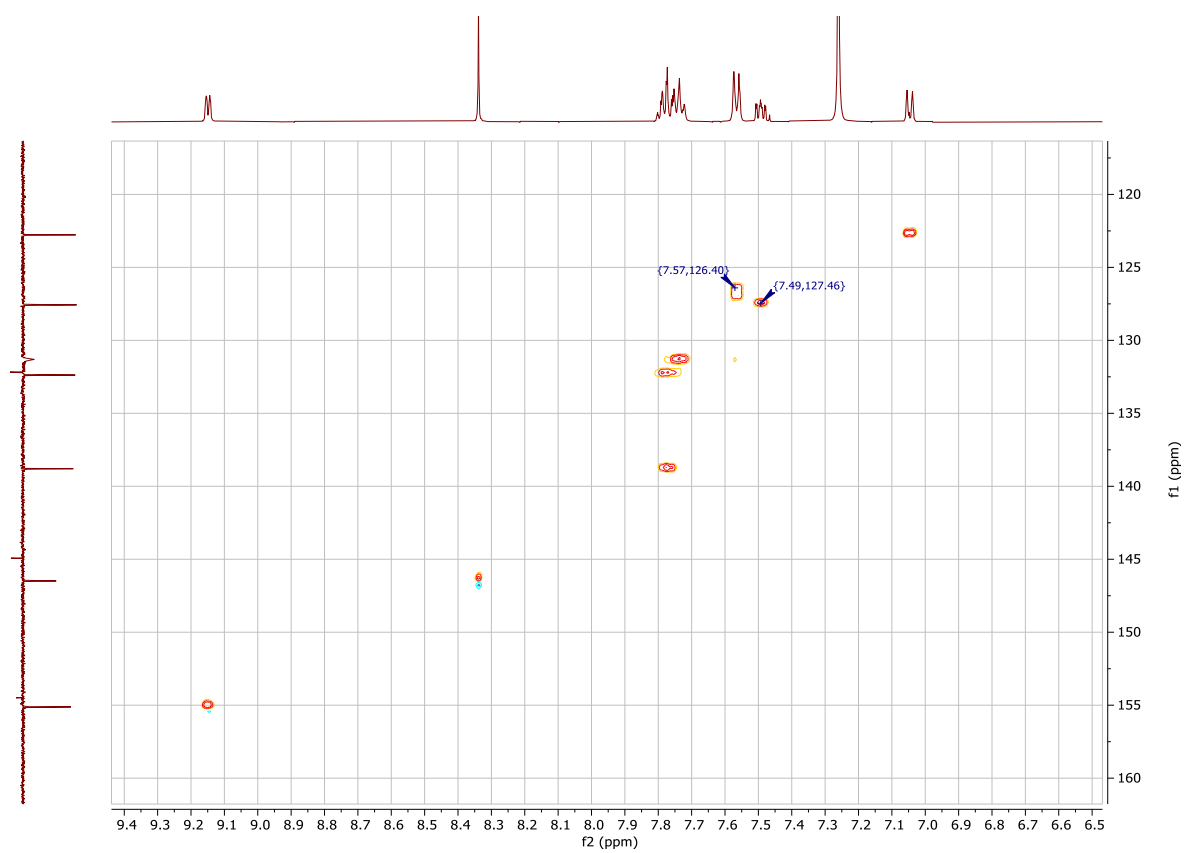
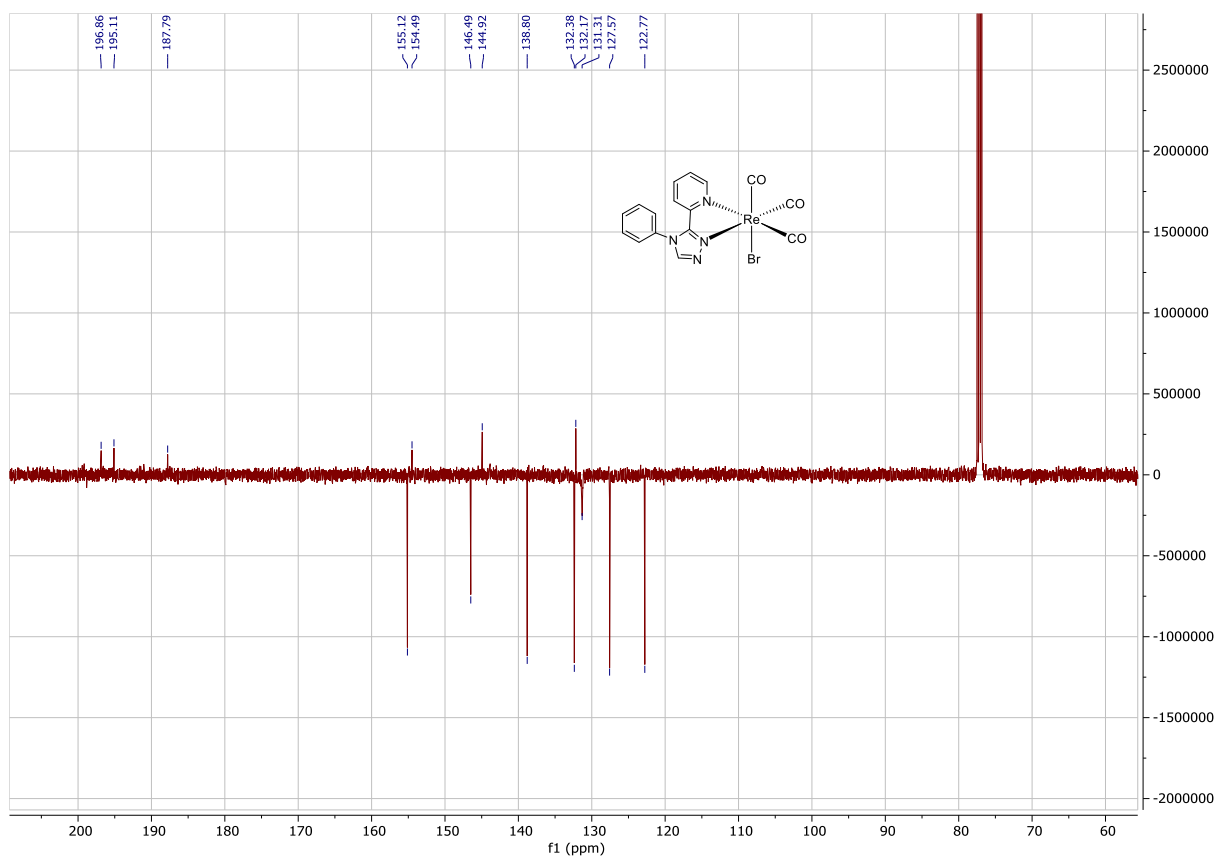


Figure S3. ¹³C NMR (top) and HSQC (bottom) spectra of complex **1-Br** in CDCl₃.

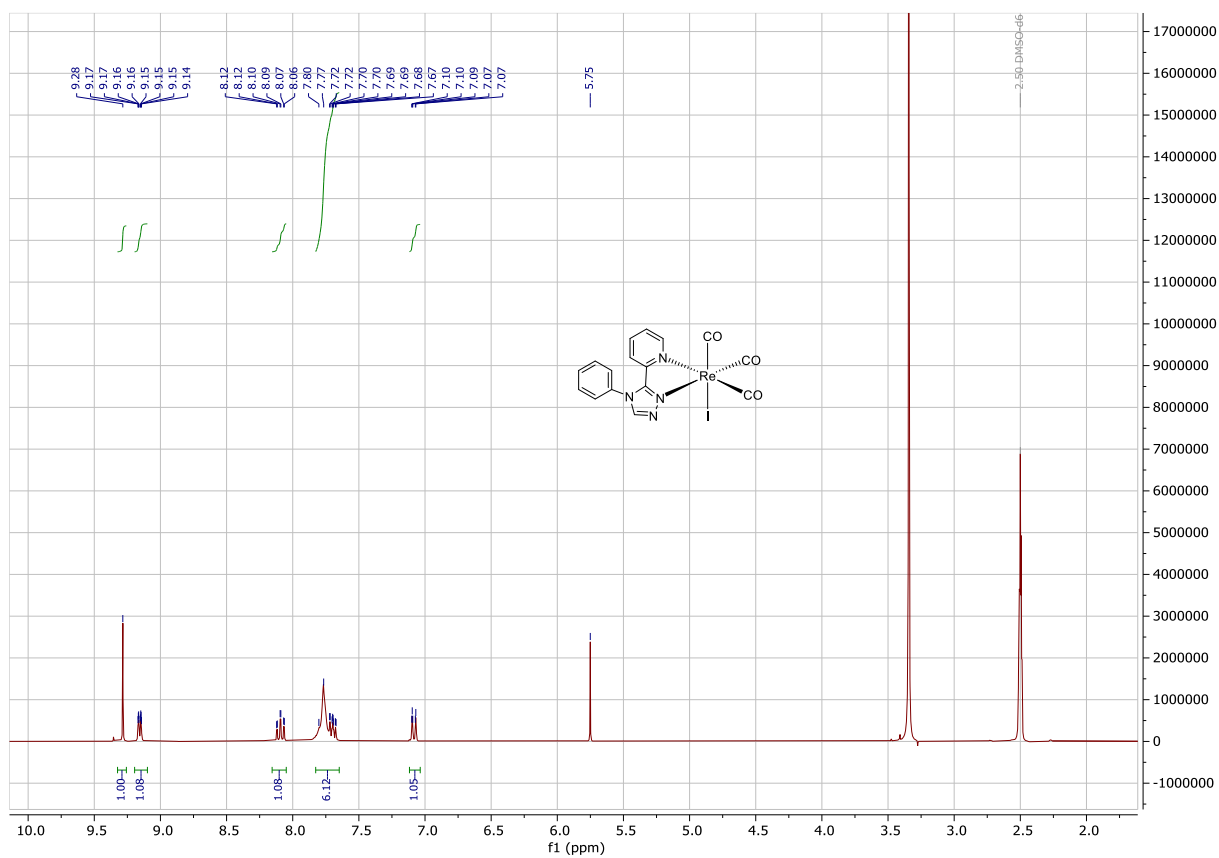
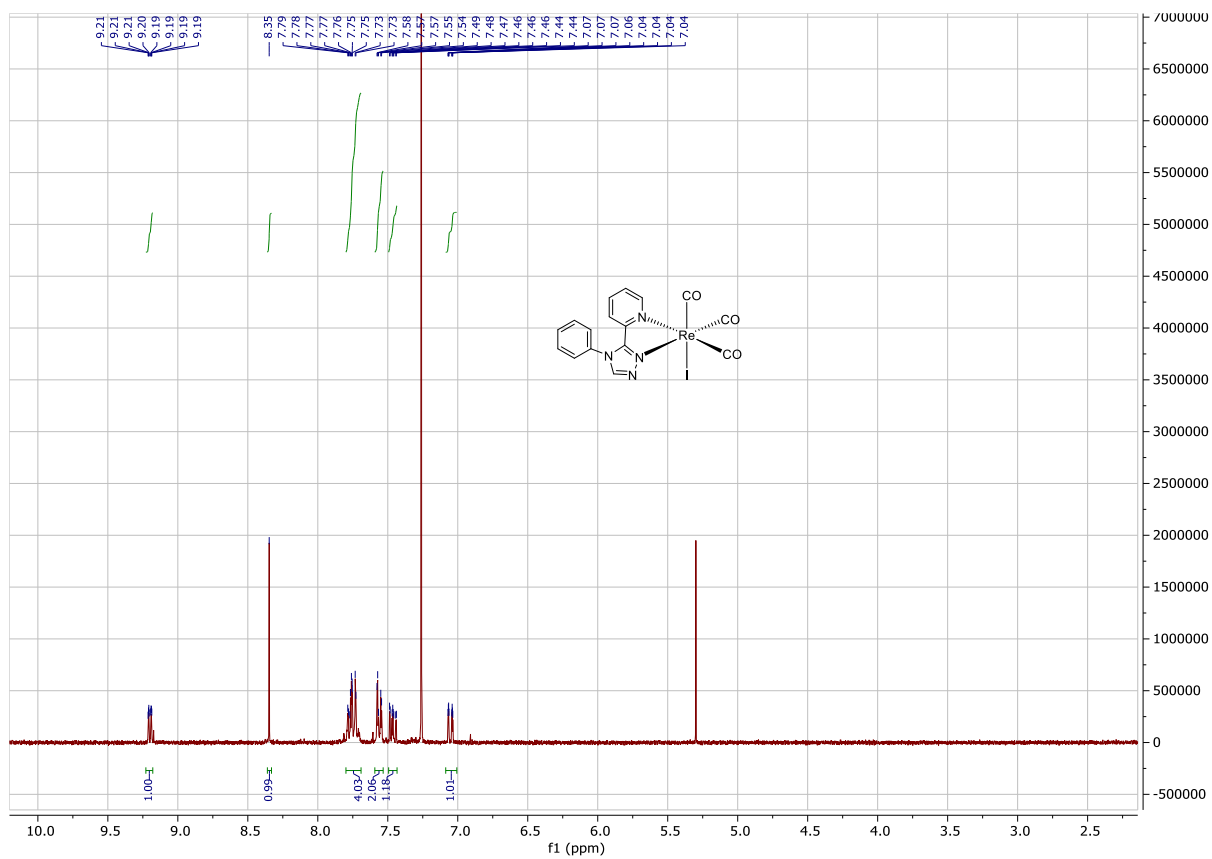


Figure S4. ^1H NMR spectra of complex 1-I in CDCl_3 (top) and DMSO-d_6 (bottom).

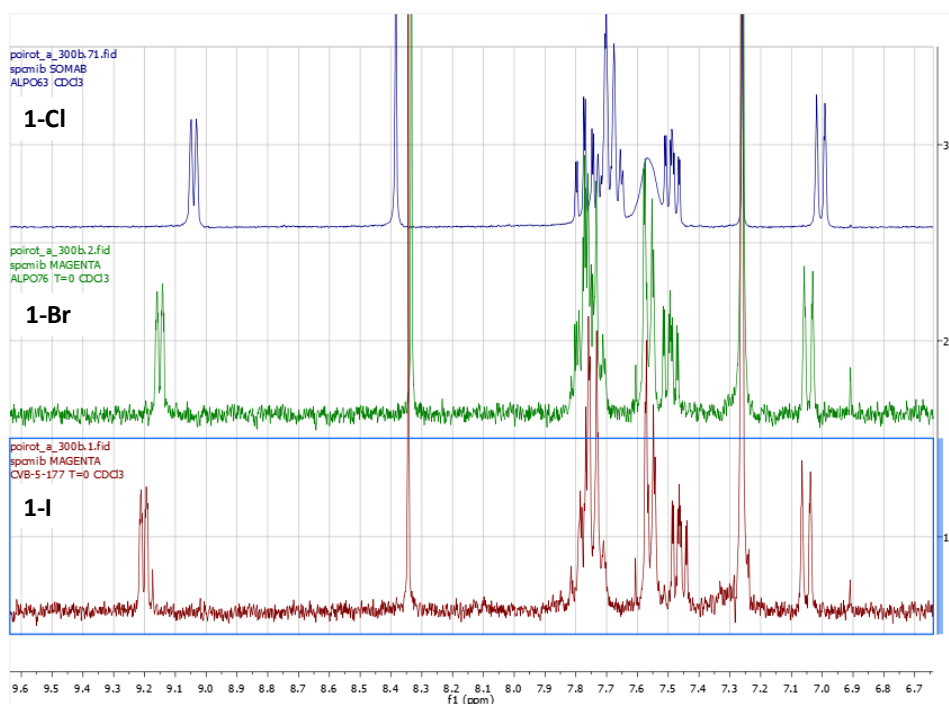


Figure S6. Comparison of the ^1H NMR spectra of complexes **1-Cl** (top), **1-Br** (middle) and **1-I** (bottom) in CDCl_3 .

Crystallographic data

Table S1. Selected bond lengths (\AA) for complexes **1-Cl**, **1-Br** and **1-I**. Data related to the second molecule of the asymmetric unit are mentioned in blue ink. The atoms were numbered like on the molecular views. For the sake of comparison, each line corresponds to the same bond in every complex.

1-Cl ^a		1-Br		1-I	
Bond	D (\AA)	Bond	D (\AA)	Bond	D (\AA)
Re1-Cl1/Re2-Cl2	2.474(2)/2.476(2)	Re1-Br1/Re2-Br2	2.6025(10)/2.6241(9)	Re1-I1/Re2-I2	2.799(6)/2.7759(9)
		Re1-Br1'/Re2-Br2'	2.490(9)/2.570(13)	Re2'-I2'	2.7790(13)
Re1-N1/Re2-N5	2.200(7)/2.191(7)	Re1-N1/Re2-N5	2.198(5)/2.206(5)	Re1-N1/Re2-N5	2.202(6)/2.200(6)
Re1-N2/Re2-N6	2.147(7)/2.157(8)	Re1-N2/Re2-N6	2.140(5)/2.150(5)	Re1-N2/Re2-N6	2.148(5)/2.139(6)
Re1-C1/Re2-C17	1.935(10)/1.899(10)	Re1-C1/Re2-C17	1.911(8)/1.918(8)	Re1-C2/Re2-C18	1.931(8)/1.907(9)
Re1-C2/Re2-C18	1.902(11)/1.900(10)	Re1-C2/Re2-C18	1.916(7)/1.918(8)	Re1-C3/Re2-C19	1.923(8)/1.942(8)
Re1-C3/Re2-C19	1.869(10)/1.895(10)	Re1-C3/Re2-C19	1.924(12)/1.920(10)	Re1-C1/Re2-C17	1.969(10)/1.883(8)
O1-C1/O4-C17	1.140(11)/1.150(10)	O1-C1/O4-C17	1.151(8)/1.160(8)	O2-C2/O5-C18	1.128(9)/1.151(10)
O2-C2/O5-C18	1.171(11)/1.148(10)	O2-C2/O5-C18	1.154(8)/1.162(8)	O3-C3/O6-C19	1.144(9)/1.126(9)
O3-C3/O6-C19	1.182(10)/1.159(10)	O3-C3/O6-C19	1.152(15)/1.144(13)	O1-C1/O4-C17	1.050(10)/1.159(8)

^a From Poirot *et al.*, *Dalton Trans.* 2021, 50, 13686–13698.

Table S2. Selected angles (°) for complexes **1-Cl**, **1-Br** and **1-I**. Data related to the second molecule of the asymmetric unit of **1** and **4** are mentioned in blue ink. The atoms were numbered like on the molecular views. For the sake of comparison, each line corresponds to the same bond in each complex.

1-Cl^a		1-Br		1-I	
Bond angle	Angle value (°)	Bond angle	Angle value (°)	Bond angle	Angle value (°)
C3-Re1-C2 / C19-Re2-C18	89.0(4) / 89.5(4)	C3-Re1-C2 / C19-Re2-C17	90.0(4) / 87.3(3)	C1-Re1-C3 / C17-Re2-C19	88.2(3) / 91.0(4)
C3-Re1-C1 / C19-Re2-C17	89.5(4) / 87.0(4)	C3-Re1-C1 / C19-Re2-C18	89.9(4) / 87.9(3)	C1-Re1-C2 / C17-Re2-C18	88.6(3) / 88.4(4)
C2-Re1-C1 / C18-Re2-C17	90.1(4) / 89.3(4)	C2-Re1-C1 / C17-Re2-C18	90.2(3) / 88.2(3)	C3-Re1-C2 / C19-Re2-C18	89.3(3) / 91.1(3)
C3-Re1-N2 / C19-Re2-N6	97.2(3) / 96.7(3)	C3-Re1-N2 / C19-Re2-N6	91.9(4) / 92.9(3)	C1-Re1-N2 / C17-Re2-N6	93.3(3) / 96.0(3)
C2-Re1-N2 / C18-Re2-N6	98.1(3) / 99.1(3)	C2-Re1-N2 / C17-Re2-N6	97.0(2) / 100.2(2)	C3-Re1-N2 / C19-Re2-N6	99.7(3) / 95.6(3)
C1-Re1-N2 / C17-Re2-N6	169.5(3) / 170.8(3)	C1-Re1-N2 / C18-Re2-N6	172.5(2) / 171.5(2)	C2-Re1-N2 / C18-Re2-N6	170.8(3) / 171.9(3)
C3-Re1-N1 / C19-Re2-N5	93.0(3) / 93.9(3)	C3-Re1-N1 / C19-Re2-N5	95.6(4) / 95.4(3)	C1-Re1-N1 / C17-Re2-N5	96.3(3) / 96.7(3)
C2-Re1-N1 / C18-Re2-N5	171.9(3) / 173.1(3)	C2-Re1-N1 / C17-Re2-N5	169.6(2) / 173.6(2)	C3-Re1-N1 / C19-Re2-N5	172.2(3) / 167.5(3)
C1-Re1-N1 / C17-Re2-N5	97.7(3) / 97.0(3)	C1-Re1-N1 / C18-Re2-N5	98.5(2) / 97.6(2)	C2-Re1-N1 / C18-Re2-N5	97.1(3) / 98.9(3)
N2-Re1-N1 / N6-Re2-N5	73.9(3) / 74.5(3)	N2-Re1-N1 / N6-Re2-N5	74.1(2) / 73.9(2)	N2-Re1-N1 / N6-Re2-N5	73.8(2) / 73.8(2)
C3-Re1-Cl1 / C19-Re2-Cl2	176.5(3) / 177.1(3)	C3-Re1-Br1 / C19-Re2-Br2	179.0(4) / 176.6(3)	C1-Re1-I1 / C17-Re2-I2	177.3(2) / 175.5(3)
C2-Re1-Cl1 / C18-Re2-Cl2	94.5(3) / 93.5(3)	C2-Re1-Br1 / C17-Re2-Br2	89.1(2) / 91.82(19)	C3-Re1-I1 / C19-Re2-I2	90.2(2) / 86.7(2)
C1-Re1-Cl1 / C17-Re2-Cl2	90.7(3) / 92.9(3)	C1-Re1-Br1 / C18-Re2-Br2	90.5(2) / 95.30(19)	C2-Re1-I1 / C18-Re2-I2	93.6(2) / 87.8(3)
N2-Re1-Cl1 / N6-Re2-Cl2	82.09(18) / 82.94(18)	N2-Re1-Br1 / N6-Re2-Br2	87.78(15) / 84.09(13)	N2-Re1-I1 / N6-Re2-I2	84.79(15) / 88.09(1)
N1-Re1-Cl1 / N5-Re2-Cl2	83.53(19) / 83.23(18)	N1-Re1-Br1 / N5-Re2-Br2	85.27(14) / 85.16(13)	N1-Re1-I1 / N5-Re2-I2	85.08(16) / 86.27(1)
O1-C1-Re1 / O4-C17-Re2	178.3(9) / 176.4(9)	O1-C1-Re1 / O5-C18-Re2	178.9(6) / 176.4(6)	O2-C2-Re1 / O5-C18-Re2	177.7(7) / 178.7(9)
O2-C2-Re1 / O5-C18-Re2	177.5(9) / 179.7(9)	O2-C2-Re1 / O4-C17-Re2	176.5(6) / 179.3(6)	O3-C3-Re1 / O6-C19-Re2	178.4(7) / 176.7(7)
O3-C3-Re1 / O6-C19-Re2	177.1(8) / 176.7(8)	O3-C3-Re1 / O6-C19-Re2	177.0(10) / 173.6(8)	O1-C1-Re1 / O4-C17-Re2	174.9(8) / 177.5(9)

^aFrom Poirot *et al.*, *Dalton Trans.* 2021, 50, 13686–13698.

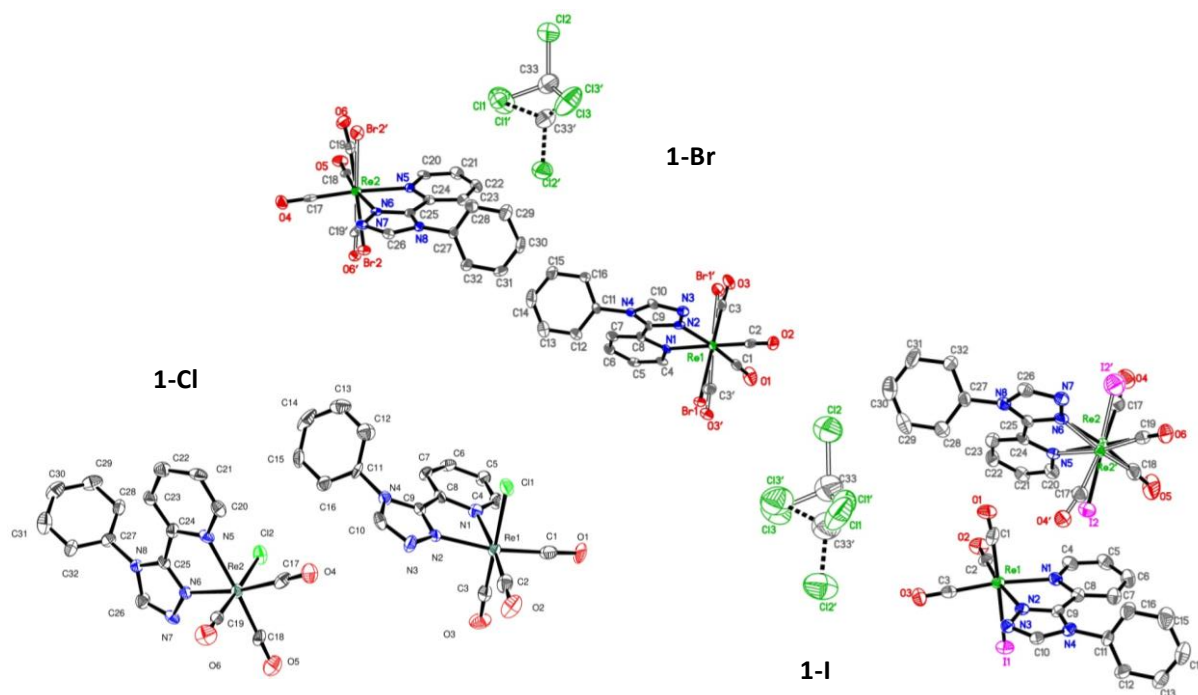


Fig. S7 Molecular view of the asymmetric unit of complexes **1-Cl**, **1-Br** and **1-I**. Hydrogen atoms are not represented for the sake of clarity. Displacement ellipsoids are drawn at 50% probability. The labels (') correspond to the minor part of the disorder, which is in every case lower than 10%.

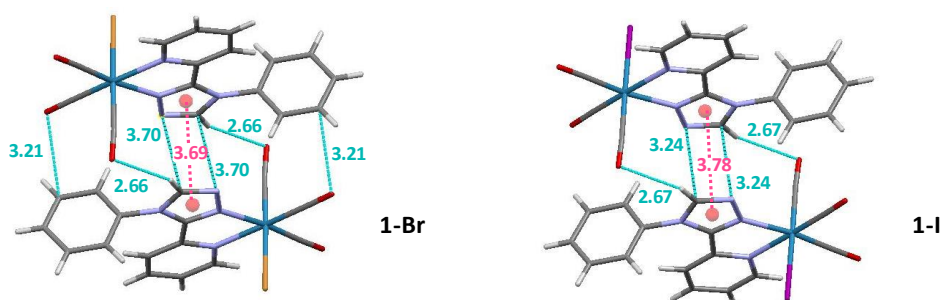


Figure S8. Crystallographic arrangement of complexes **1-Br** and **1-I** showing the relative position of two neighboring molecules. The distances in Å between the center-of-gravity Cg of the numbered rings (indicated by a pink ball) are in pink ink. Short contacts involving either the CO ligands or the nitrogen atom of the triazole moiety are indicated in blue ink.

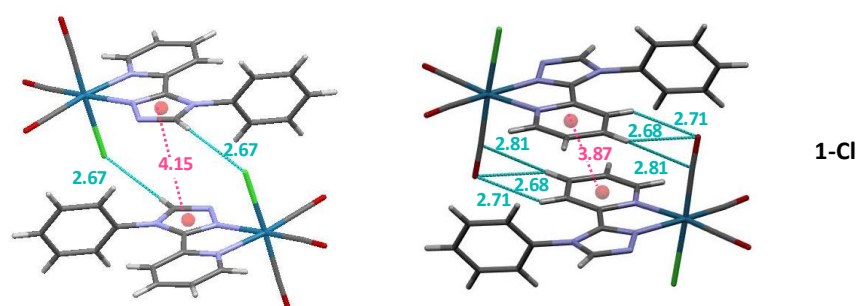


Figure S9. Crystallographic arrangement of complex **1-Cl** (from Poirot *et al.*, *Dalton Trans.* 50, 13686–13698, 2021) showing the relative position of two neighboring molecules. The distances in Å between the center-of-gravity Cg of the numbered rings (indicated by a pink ball) are in pink ink. Short contacts involving either the chlorine atoms or the CO ligand are indicated in blue ink.

Quantum chemistry calculations

Table S3. Composition (%) of the frontier molecular orbitals involved in the main electronic transitions of complex **1-Cl** in CH₂Cl₂.

	Rhenium	Cl	Pyta	Phenyl	CO
HOMO-13	11.68	21.74	58.68	3.16	4.74
HOMO-11	10.93	71.92	4.67	0.20	12.29
HOMO-8	0.50	0.42	96.68	2.22	1.18
HOMO-7	2.52	1.60	85.58	0.63	9.66
HOMO-5	6.13	20.82	4.97	65.58	2.50
HOMO-4	11.40	41.51	9.54	32.92	4.63
HOMO-3	5.68	47.12	43.69	0.68	2.82
HOMO-2	68.17	0.55	1.38	0.09	29.81
HOMO-1	45.70	28.61	5.14	0.06	20.49
HOMO	47.44	25.37	4.45	0.066	22.68
LUMO	2.69	1.74	89.75	0.49	5.328
LUMO+1	0.33	0.14	94.85	3.01	1.67
LUMO+2	17.09	0.80	1.86	16.03	64.22
LUMO+3	8.23	1.22	6.00	59.84	24.70
LUMO+4	13.49	1.96	8.87	23.05	52.63
LUMO+5	1.63	0.18	12.29	79.79	6.11
LUMO+7	0.54	0.17	20.00	1.82	77.46
LUMO+10	34.89	0.32	8.32	0.34	56.13

Table S4. Description of the main electronic transitions for complex **1-Cl** in CH₂Cl₂ calculated using the TD-DFT method at the PBE0/LANL2DZ level, with corresponding wavelength (λ), energy (E) and oscillator strength (f). Assignments have been revisited with respect to Poirot *et al.*, *Dalton Trans.* 2021, 50, 13686–13698, according to the frontier molecular orbital composition. Only orbitals contributing by more than 5% have been indicated, and they are listed in decreasing order of importance.

Electronic transition	Contribution	Assignment	Character	λ (nm)	E (eV)	f
S ₀ →S ₂	H-1→LUMO	d(Re)+p(Cl)+ π (CO)+ π (Pyta)→ π^* (Pyta)+ π^* (CO)	MLCT/XLCT	418.2	2.97	0.0919
S ₀ →S ₁₀	H-4→LUMO H-5→LUMO	p(Cl)+ π (Phe)+d(Re)→ π^* (Pyta)+ π^* (CO) π (Phe)+p(Cl)+d(Re)→ π^* (Pyta)+ π^* (CO)	XLCT/LLCT/MLCT ILCT/XLCT/MLCT	305.3	4.06	0.0925
S ₀ →S ₂₀	H-7→LUMO	π (Pyta)+ π (CO)→ π^* (Pyta)+ π^* (CO)	IL	254.2	4.88	0.1057
S ₀ →S ₂₁	H-2→L+2 H-1→L+7 H-7→LUMO	d(Re)+ π (CO)→ π^* (CO)+p(Re)+ π^* (Phe) d(Re)+p(Cl)+ π (CO)+ π (Pyta)→ π^* (CO)+ π^* (Pyta) π (Pyta)+ π (CO)→ π^* (Pyta)+ π^* (CO)	MLCT MLCT/XLCT/IL IL	251.4	4.93	0.0742
S ₀ →S ₂₁	H-3→L+1	p(Cl)+ π (Pyta)+d(Re)→ π^* (Pyta)	XLCT/IL/MLCT	248.8	4.98	0.0435
S ₀ →S ₂₄	H-1→L+5 H-8→LUMO	d(Re)+p(Cl)+ π (CO)+ π (Pyta)→ π^* (Phe)+ π^* (Pyta)+ π^* (CO) π (Pyta)→ π^* (Pyta)+ π^* (CO)	MLCT/XLCT/LLCT IL/LLCT	243.4	5.09	0.0424
S ₀ →S ₃₀	H-5→L+1	π (Phe)+p(Cl)+d(Re)→ π^* (Pyta)	ILCT/XLCT/MLCT	232.7	5.33	0.0522
S ₀ →S ₄₈	H-1→L+10 H-3→L+4	d(Re)+p(Cl)+ π (CO)+ π (Pyta)→ π^* (CO)+p(Re)+ π^* (Pyta) p(Cl)+ π (Pyta)+d(Re)→ π^* (CO)+ π^* (Phe)+p(Re)	MLCT/XLCT XLCT/LLCT/ILCT	213.2	5.82	0.0799
S ₀ →S ₅₄	H-13→LUMO H-2→L+10	π (Pyta)+p(Cl)+d(Re)→ π^* (Pyta)+ π^* (CO) d(Re)+ π (CO)→ π^* (CO)+p(Re)+ π^* (Pyta)	IL/XLCT/MLCT MLCT	202.7	6.12	0.0488
S ₀ →S ₅₈	H-11→LUMO	p(Cl)+ π (CO)+d(Re)→ π^* (Pyta)+ π^* (CO)	XLCT/MLCT	197.1	6.29	0.0300

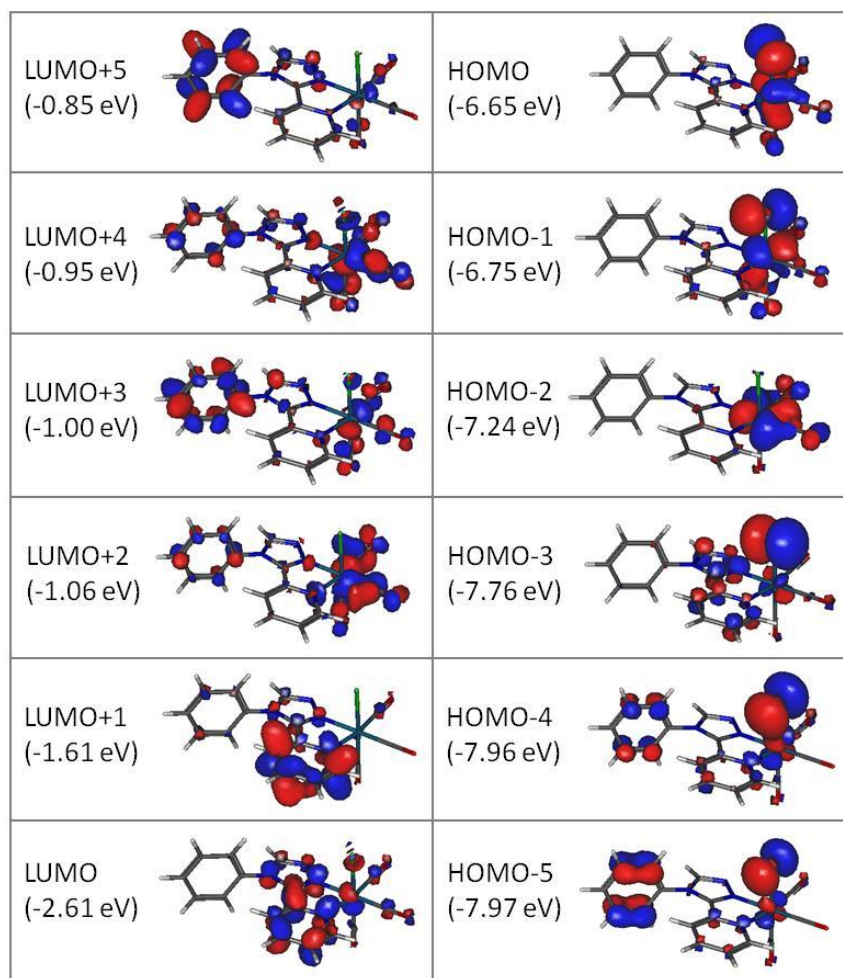


Figure S10. Energy levels and isodensity plots (isovalue = 0.03) of the first frontier molecular orbitals of complex **1-Cl** in dichloromethane, according to DFT calculations at the PBE0/LANL2DZ level of theory.

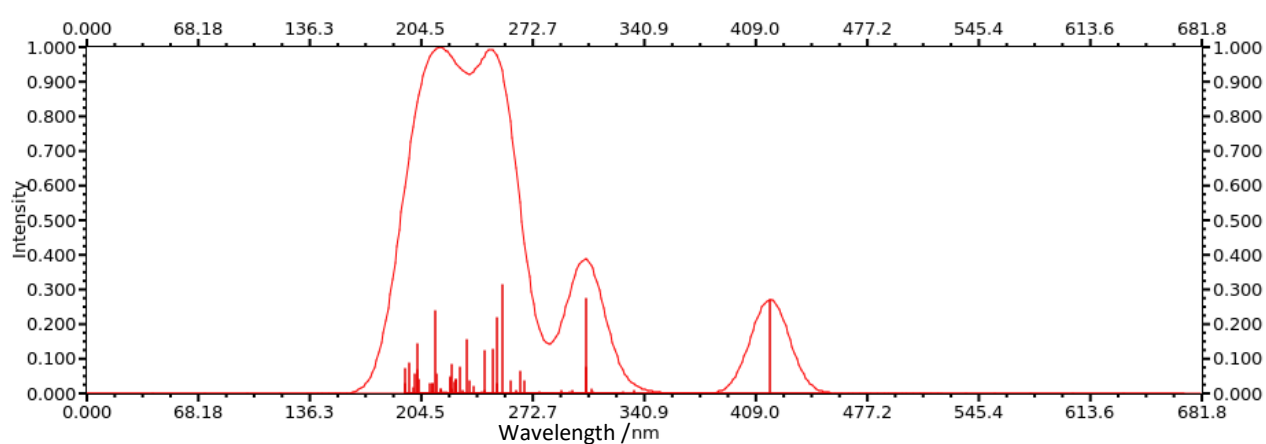


Figure S11. Theoretical UV-vis absorption spectrum and main electronic transitions for complex **1-Cl** in CH_2Cl_2 calculated using the TD-DFT method at the PBE0/LANL2DZ level (From ref. Poirot *et al.*, *Dalton Trans.* 2021, 50, 13686–13698).

Table S5. Composition (%) of the frontier molecular orbitals involved in the main electronic transitions of complex **1-Br** in CH₂Cl₂.

	Rhenium	Br	Pyta	Phenyl	CO
HOMO-11	0.50	0.26	97.26	1.84	0.15
HOMO-8	13.10	64.60	10.25	0.26	11.79
HOMO-7	10.98	9.98	70.91	3.10	5.03
HOMO-6	0.30	0.02	9.46	89.99	0.23
HOMO-5	0.06	0.04	1.75	98.13	0.03
HOMO-4	27.34	49.75	11.57	0.07	11.26
HOMO-3	16.72	51.04	24.46	0.30	7.48
HOMO-2	68.20	0.52	1.40	0.0	29.80
HOMO-1	35.00	45.62	3.82	0.04	15.52
HOMO	37.81	41.02	3.10	0.05	18.02
LUMO	2.58	2.46	89.18	0.49	5.30
LUMO+1	0.38	0.19	94.79	2.94	1.71
LUMO+2	19.82	1.04	1.65	7.76	69.73
LUMO+3	12.43	3.17	7.66	37.79	38.95
LUMO+4	8.01	1.58	5.98	51.84	32.58
LUMO+5	1.02	0.15	13.78	80.86	4.19
LUMO+8	31.21	1.14	23.68	0.29	43.67
LUMO+10	32.93	0.92	9.76	0.36	56.03
LUMO+12	66.44	0.92	6.41	0.09	26.14

Table S6. Description of the main electronic transitions for complex **1-Br** in CH₂Cl₂ calculated using the TD-DFT method at the PBEO/LANL2DZ level, with corresponding wavelength (λ), energy (E) and oscillator strength (f). Only orbitals contributing by more than 5% have been indicated, and they are listed in decreasing order of importance.

Electronic transition	Contribution	Assignment	Character	λ (nm)	E (eV)	f
S ₀ → S ₂	H-1 → LUMO	p(Br)+d(Re)+ π (CO) → π^* (Pyta)+ π^* (CO)	XLCT/MLCT	443.8	2.79	0.0625
S ₀ → S ₄	H-3 → LUMO	p(Br)+ π (Pyta)+d(Re)+ π (CO) → π^* (Pyta)+ π^* (CO)	XLCT/IL/MLCT	340.7	3.64	0.0242
S ₀ → S ₆	H-1 → L+1	p(Br)+d(Re)+ π (CO) → π^* (Pyta)	XLCT/MLCT	332.4	3.73	0.0435
S ₀ → S ₈	HOMO → L+1	p(Br)+d(Re)+ π (CO) → π^* (Pyta)	XLCT/MLCT	325	3.82	0.0518
S ₀ → S ₂₀	H-7 → LUMO	π (Pyta)+d(Re)+p(Br)+ π (CO) → π^* (Pyta)+ π^* (CO)	IL/MLCT/XLCT	264.3	4.69	0.0831
S ₀ → S ₂₁	H-8 → LUMO	p(Br)+d(Re)+ π (CO)+ π (Pyta) → π^* (Pyta)+ π^* (CO)	XLCT/MLCT	258.4	4.80	0.0446
S ₀ → S ₂₄	H-8 → LUMO H-2 → L+2	p(Br)+d(Re)+ π (CO)+ π (Pyta) → π^* (Pyta)+ π^* (CO) d(Re)+ π (CO) → π^* (CO)+p(Re)+ π^* (Phe)	XLCT/MLCT MLCT	255.4	4.86	0.0537
S ₀ → S ₂₇	H-3 → L+2 H-3 → L+3	p(Br)+ π (Pyta)+d(Re)+ π (CO) → π^* (CO)+p(Re)+ π^* (Phe) p(Br)+ π (Pyta)+d(Re)+ π (CO) → π^* (CO)+ π^* (Phe)+p(Re)	XLCT/LLCT XLCT/LLCT	245.3	5.06	0.0238
S ₀ → S ₂₈	H-3 → L+2	p(Br)+ π (Pyta)+d(Re)+ π (CO) → π^* (CO)+p(Re)+ π^* (Phe)	XLCT/LLCT	243.6	5.09	0.0470
S ₀ → S ₃₀	H-4 → L+1 H-3 → L+2	p(Br)+d(Re)+ π (Pyta)+ π^* (CO) → π^* (Pyta) p(Br)+ π (Pyta)+d(Re)+ π (CO) → π^* (CO)+p(Re)+ π^* (Phe)	XLCT/MLCT XLCT/LLCT	242.2	5.12	0.0789
S ₀ → S ₃₁	HOMO → L+8	p(Br)+d(Re)+ π (CO) → π^* (CO)+p(Re)+ π^* (Pyta)	XLCT/MLCT	241.2	5.14	0.0451
S ₀ → S ₄₄	H-8 → L+1	p(Br)+d(Re)+ π (CO)+ π (Pyta) → π^* (Pyta)	XLCT/MLCT	220.6	5.62	0.0456
S ₀ → S ₄₆	H-6 → L+1	π (Phe)+ π (Pyta) → π^* (Pyta)	ILCT	220.1	5.63	0.0353

$S_0 \rightarrow S_{51}$	H-1 \rightarrow L+10	$p(\text{Br})+d(\text{Re})+\pi(\text{CO}) \rightarrow \pi^*(\text{CO})+p(\text{Re})+\pi^*(\text{Pyta})$	XLCT	209.6	5.92	0.0531
$S_0 \rightarrow S_{60}$	HOMO \rightarrow L+12 H-11 \rightarrow LUMO	$p(\text{Br})+d(\text{Re})+\pi(\text{CO}) \rightarrow p(\text{Re})+\pi^*(\text{CO})+\pi^*(\text{Pyta})$ $\pi(\text{Pyta}) \rightarrow \pi^*(\text{Pyta})+\pi^*(\text{CO})$	XMCT/XLCT IL/LLCT	198.8	6.24	0.0386

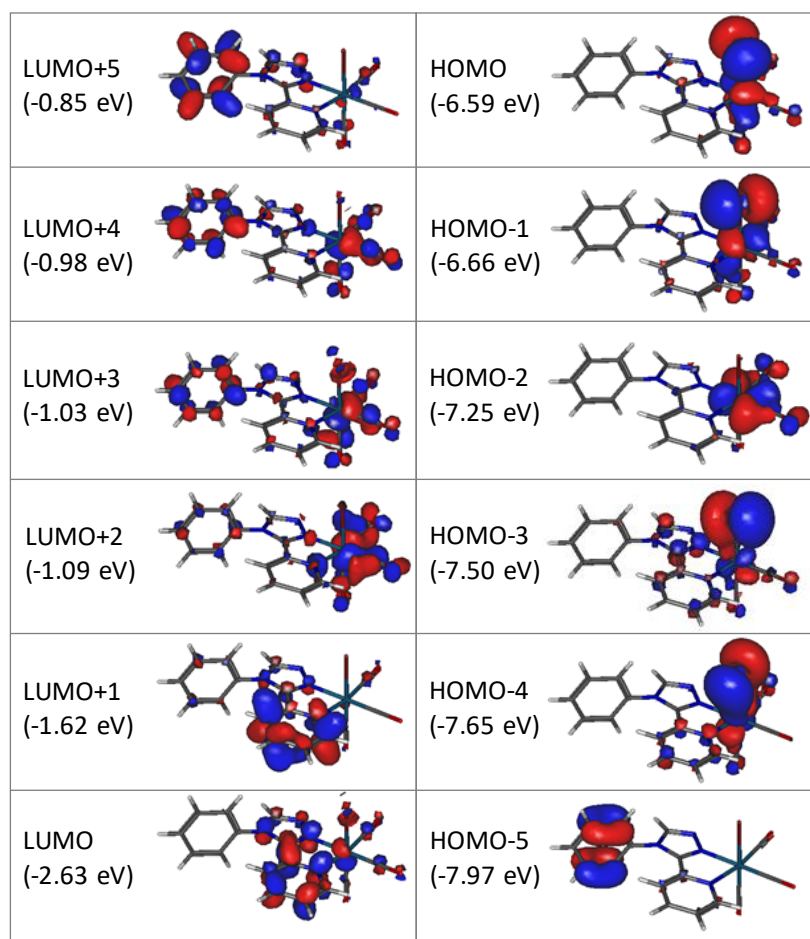


Figure S12. Energy levels and isodensity plots (isovalue = 0.03) of the first frontier molecular orbitals of complex **1-Br** in dichloromethane, according to DFT calculations at the PBE0/LANL2DZ level of theory.

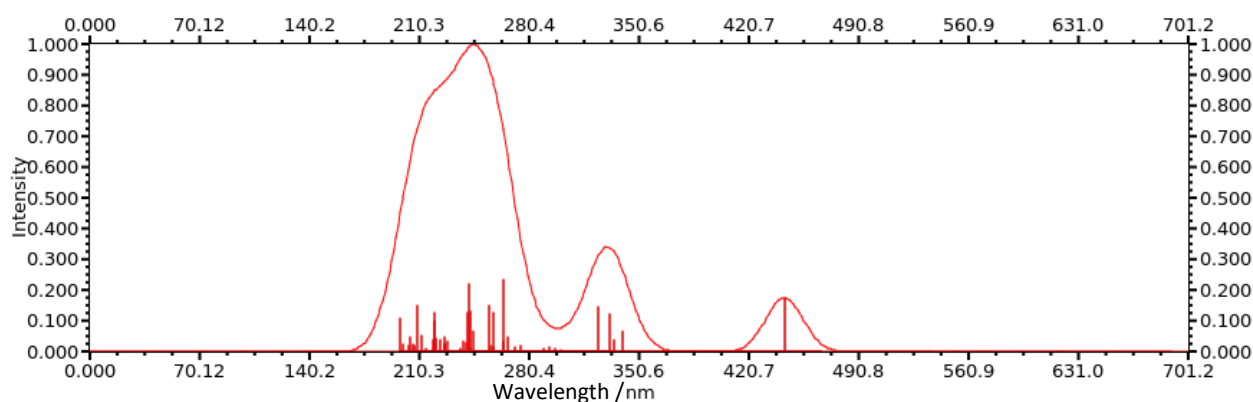


Figure S13. Theoretical UV-vis absorption spectrum and main electronic transitions for complex **1-Br** in CH_2Cl_2 calculated using the TD-DFT method at the PBE0/LANL2DZ level.

Table S7. Composition (%) of the frontier molecular orbitals involved in the main electronic transitions of complex **1-I** in CH₂Cl₂.

	Rhenium	I	Pyta	Phenyl	CO
HOMO-13	2.69	0.55	86.43	0.65	9.68
HOMO-8	6.19	2.51	74.49	14.73	2.08
HOMO-5	25.89	57.01	0.55	0.17	16.37
HOMO-4	39.37	32.27	11.40	0.03	16.93
HOMO-3	55.59	12.89	7.16	0.30	24.07
HOMO-2	39.95	28.05	14.28	0.22	17.50
HOMO-1	21.81	66.45	2.26	0.03	9.45
HOMO	23.78	63.60	1.40	0.02	11.21
LUMO	2.46	3.34	88.59	0.60	5.018
LUMO+1	0.46	0.28	94.12	3.38	1.76
LUMO+2	21.90	1.17	1.12	3.52	72.28
LUMO+3	15.91	5.44	9.33	21.00	48.32
LUMO+4	4.67	1.21	4.93	71.13	18.06
LUMO+5	0.80	0.14	13.59	82.14	3.33
LUMO+6	1.39	0.14	46.71	11.22	40.54

Table S8. Description of the main electronic transitions for complex **1-I** in CH₂Cl₂ calculated using the TD-DFT method at the PBE0/LANL2DZ level, with corresponding wavelength (λ), energy (E) and oscillator strength (f). Only orbitals contributing by more than 5% have been indicated, and they are listed in decreasing order of importance.

Electronic transition	Contribution	Assignment		λ (nm)	E (eV)	f
S ₀ →S ₂	H-1→LUMO	p(I)+d(Re)+ π (CO)→ π^* (Pyta)+ π^* (CO)	XLCT/MLCT	498.4	2.49	0.0340
S ₀ →S ₅	H→LUMO+1	p(I)+d(Re)+ π (CO)→ π^* (Pyta)	XLCT/MLCT/LLCT	363.9	3.41	0.0464
S ₀ →S ₆	H-2→LUMO H-3→LUMO	d(Re)+p(I)+ π (CO)+ π (Pyta)→ π^* (Pyta)+ π^* (CO) d(Re)+ π (CO)+p(I)+ π (Pyta)→ π^* (Pyta)+ π^* (CO)	MLCT/XLCT/LLCT MLCT/LLCT/XLCT	356.5	3.48	0.0362
S ₀ →S ₇	H-4→LUMO	d(Re)+p(I)+ π (CO)+ π (Pyta)→ π^* (Pyta)+ π^* (CO)	MLCT/XLCT/LLCT	344.2	3.60	0.0705
S ₀ →S ₁₆	H-5→LUMO+1	p(I)+d(Re)+ π (CO)→ π^* (Pyta)	XLCT/MLCT/LLCT	287.4	4.31	0.0517
S ₀ →S ₂₁	H-2→LUMO+1	d(Re)+p(I)+ π (CO)+ π (Pyta)→ π^* (Pyta)	MLCT/XLCT/LLCT	268.2	4.62	0.0264
S ₀ →S ₂₂	H-8→LUMO	π (Pyta)+ π (Phe)+d(Re)→ π^* (Pyta)+ π^* (CO)	ILCT/MLCT/LLCT	267.3	4.64	0.0537
S ₀ →S ₂₉	H-4→LUMO+3 H-4→LUMO+1	d(Re)+p(I)+ π (CO)+ π (Pyta)→ π^* (CO)+ π^* (Phe)+p(Re)+ π^* (Pyta)+p(I) d(Re)+p(I)+ π (CO)+ π (Pyta)→ π^* (Pyta)	MLCT/XLCT MLCT/XLCT/LLCT	247.7	5.01	0.0535
S ₀ →S ₃₁	H-4→LUMO+1	d(Re)+p(I)+ π (CO)+ π (Pyta)→ π^* (Pyta)	MLCT/XLCT/LLCT	245	5.06	0.1280
S ₀ →S ₃₇	H→LUMO+6	p(I)+d(Re)+ π (CO)→ π^* (Pyta)+ π^* (CO)+ π^* (Phe)	XLCT/MLCT	238.1	5.21	0.0514
S ₀ →S ₄₆	H-2→LUMO+5	d(Re)+p(I)+ π (CO)+ π (Pyta)→ π^* (Phe)+ π^* (Pyta)	MLCT/XLCT/LLCT	222.7	5.57	0.0727
S ₀ →S ₅₁	H-8→LUMO+1	π (Pyta)+ π (Phe)+d(Re)→ π^* (Pyta)	ILCT/MLCT	218.5	5.68	0.0282
S ₀ →S ₅₃	H-4→LUMO+3	d(Re)+p(I)+ π (CO)+ π (Pyta)→ π^* (CO)+ π^* (Phe)+p(Re)+ π^* (Pyta)+p(I)	XLCT/MLCT	215.5	5.75	0.0571
S ₀ →S ₅₉	H-13→LUMO	π (Pyta)+ π (CO)→ π^* (Pyta)+ π^* (CO)	IL	203.9	6.08	0.0734

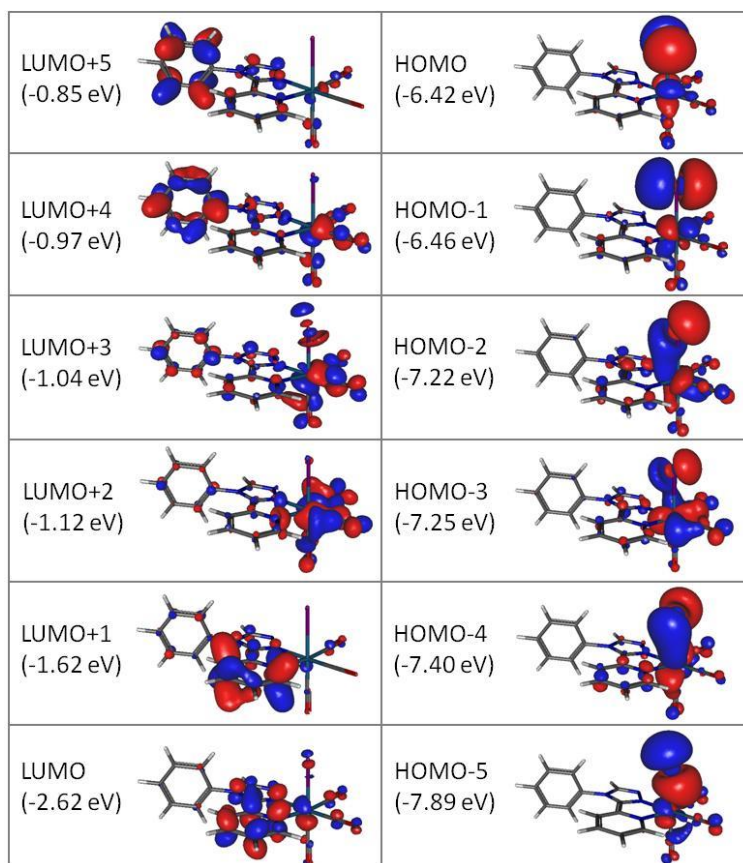


Figure S14. Energy levels and isodensity plots (isovalue = 0.03) of the first frontier molecular orbitals of complex **1-I** in dichloromethane, according to DFT calculations at the PBE0/LANL2DZ level of theory.

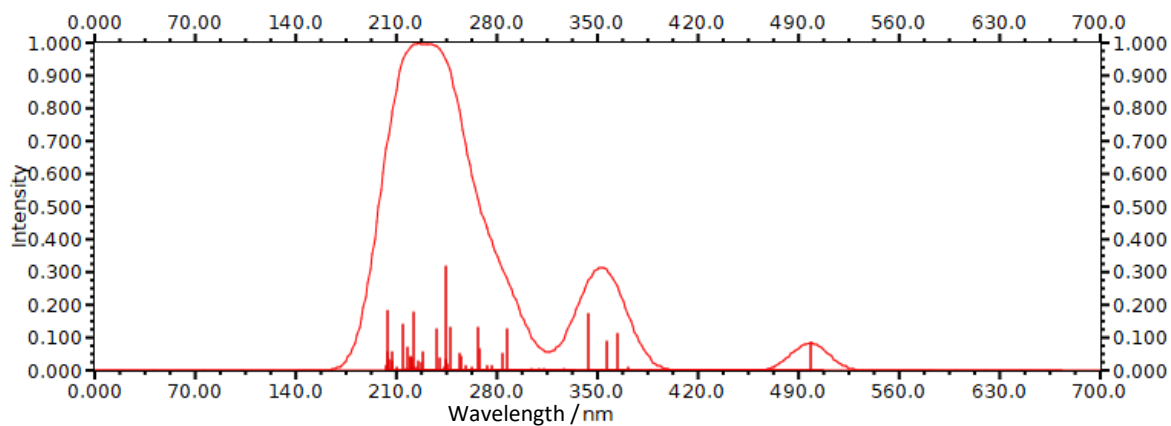


Figure S15. Theoretical UV-vis absorption spectrum and main electronic transitions for complex **1-I** in CH_2Cl_2 calculated using the TD-DFT method at the PBE0/LANL2DZ level.

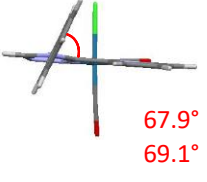
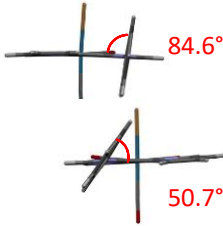
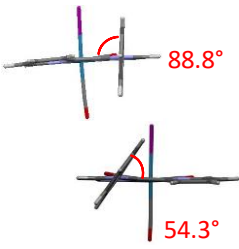
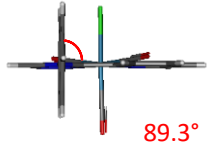
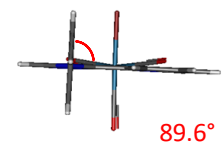
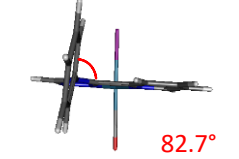
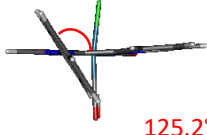
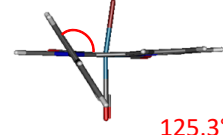
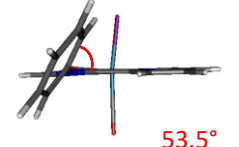
	1-Cl	1-Br	1-I
Crystals			
Ground state			
First triplet excited state			

Figure S16. Geometry and phenyl-pyta dihedral angle values of complexes **1-Cl**, **1-Br** and **1-I** in the crystal (crystallography data), and in the ground and first triplet excited state (TD-DFT).

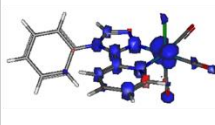
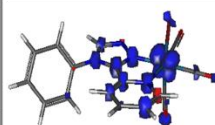
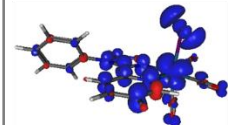
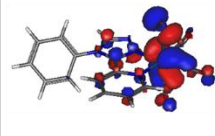
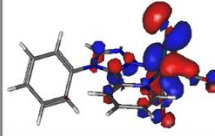
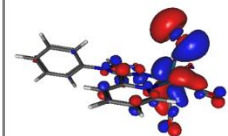
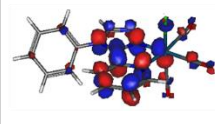
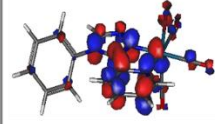
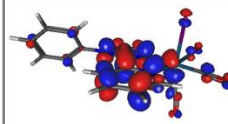
	1-Cl	1-Br	1-I
Spin density			
Hole (HOMO)			
Particle (LUMO)			

Figure S17. Representation of the spin density and position of unpaired electrons in the triplet state of **1-Cl**, **1-Br** and **1-I** (isovalue = 0.03). Data obtained from the comparison of the Kohn-Sham orbitals of the molecules in the triplet state with those of the ground state.

Electrochemistry

Table S9. Selected electrochemical data of complexes **1-Cl**, **1-Br** and **1-I** [1.0×10^{-3} M]. Values determined by OSWV on a Pt working electrode in $\text{CH}_2\text{Cl}_2 + 0.1$ M *n*-Bu₄NBF₄ at room temperature.^{a,b} Ferrocene was used as internal reference.

Compound	Oxidation			Reduction	
	E_3	E_2	E_1	E_1	E_2^g
1-Cl ^h	1.78	---	1.46	-1.29 ^c	-1.78
1-Br	1.77	---	1.43 ^d	-1.31 ^e	-1.88
1-I	1.78	1.48	1.26	-1.27 ^f	-1.91

^a OSWVs were obtained using a sweep width of 20 mV, a frequency of 20 Hz, and a step potential of 5 mV.

^b Potential values in Volts vs. SCE (Fc⁺/Fc is observed at 0.55 V \pm 0.01 V vs. SCE).

^c One-electron quasi-reversible process at 1.0 V/s.

^d This process presents some slightly reversible character at 50 V/s.

^e Quasi-reversible process at 5 V/s.

^f This process presents some slightly reversible character at 50 V/s

^g This process has a weak intensity when compared to the E_1 reduction process or appears as a shoulder.

^h From, A. Poirot *et al.*, *Dalton Trans.*, 2021, 50, 13686–13698.

Table S10. Experimental electrochemical data used, and calculated values of the energy gaps (E_g) for complexes **1-Cl**, **1-Br** and **1-I**.

Compound	$E_{\text{onset ox}}$ (V)	$E_{\text{onset red}}$ (V)	E_{HOMO} (eV)	E_{LUMO} (eV)	E_g^{el} (eV)	$E_{\text{calc}}^{\text{a}}$ (eV)
1-Cl	1.42	-1.23	-6.16	-3.51	2.65	2.73 ^b
1-Br	1.39	-1.22	-6.13	-3.52	2.61	2.65
1-I	1.14	-1.17	-5.88	-3.57	2.31	2.42

^a The values were obtained using the TD-DFT method and considering the optimized geometry of the S_1 state.

^b From, A. Poirot *et al.*, *Dalton Trans.*, 2021, 50, 13686–13698.

Evaluation of the energy gap values (E_g^{el}) for the Re complexes.

The onset oxidation and reduction potentials ($E_{\text{onset ox}}$, $E_{\text{onset red}}$) were measured by cyclic voltammetry in volt *versus* SCE. The CVs were carried out at a potential scan rate of 200 mV s⁻¹ at room temperature.

The HOMO and LUMO energy levels (E_{HOMO} and E_{LUMO}) in electron volt (eV) were calculated according to the empirical equations (1) and (2):^[1]

$$E_{\text{HOMO}} (\text{eV}) = -e (E_{\text{onset ox}} (\text{V vs. SCE}) + 4.74 \text{ V}) \quad \text{Eq(1)}$$

$$E_{\text{LUMO}} (\text{eV}) = -e (E_{\text{onset red}} (\text{V vs. SCE}) + 4.74 \text{ V}) \quad \text{Eq(2)}$$

and the energy gap value was obtained as follows: $E_g^{\text{el}} = (E_{\text{LUMO}} - E_{\text{HOMO}})$.

The differences observed for the estimation of the energy gaps using experimental methods or theoretical calculations are well known. See for example: R. Stowasser, R. Hoffmann, *J. Am. Chem. Soc.* 1999, 121, 3414-3420.

[1] a) Y. Zhou, J. W. Kim, R. Nandhakumar, M. J. Kim, E. Cho, Y. S. Kim, Y. H. Jang, C. Lee, S. Han, K. M. Kim, J.-J. Kim and J. Yoon, *Chem. Commun.* 2010, 46, 6512-6514 and references therein; b) G. V. Loukova, *Chem. Phys. Lett.* 2002, 353, 244–252.

Electrochemical selected curves

OSWV study was performed on a Pt working electrode in $\text{CH}_2\text{Cl}_2 + 0.1 \text{ M } n[\text{Bu}_4\text{N}][\text{BF}_4]$ at room temperature in the presence of ferrocene used as internal reference. Frequency 20 Hz, amplitude 20 mV, step potential 5 mV.

Cyclic voltammograms of the indicated compounds were performed on a Pt working electrode in $\text{CH}_2\text{Cl}_2 + 0.1 \text{ M } n[\text{Bu}_4\text{N}][\text{BF}_4]$ at room temperature at a scan rate of 0.2 V s^{-1} or at other mentioned scan rates.

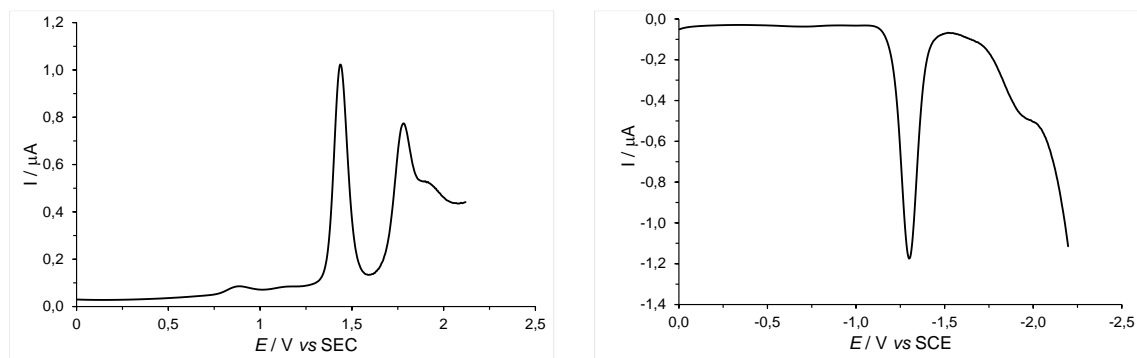


Figure S18. OSWVs: anodic (left) and cathodic (right) scans of complex **1-Br**.

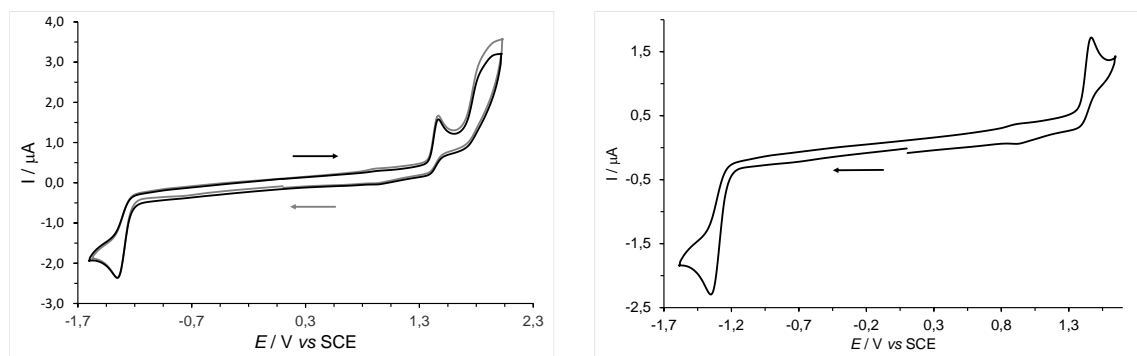


Figure S19. Cyclic voltammograms of complex **1-Br** (left), and of its first oxidation and reduction processes (right).

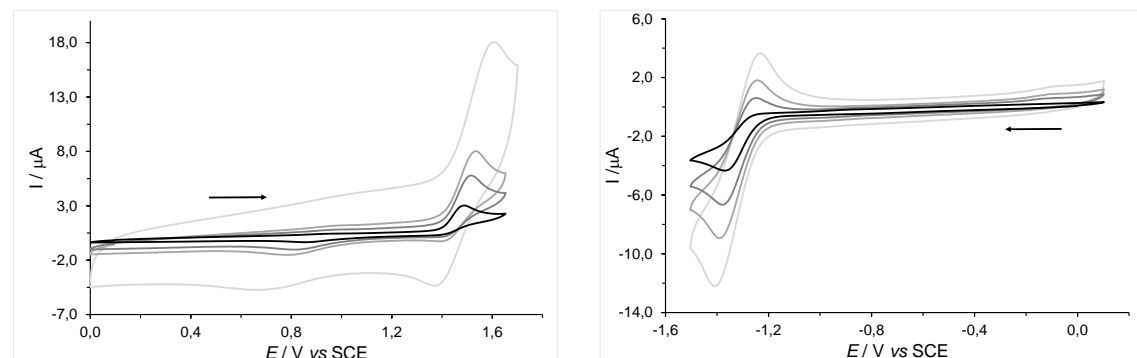


Figure S20. Complex **1-Br**: Cyclic voltammograms of the first oxidation process at 1, 5, 10, 50 V/s from bottom-black line to top-grey line (left), and of the first reduction process at 1, 5, 10, 20 V/s from bottom-black line to top-grey line (right).

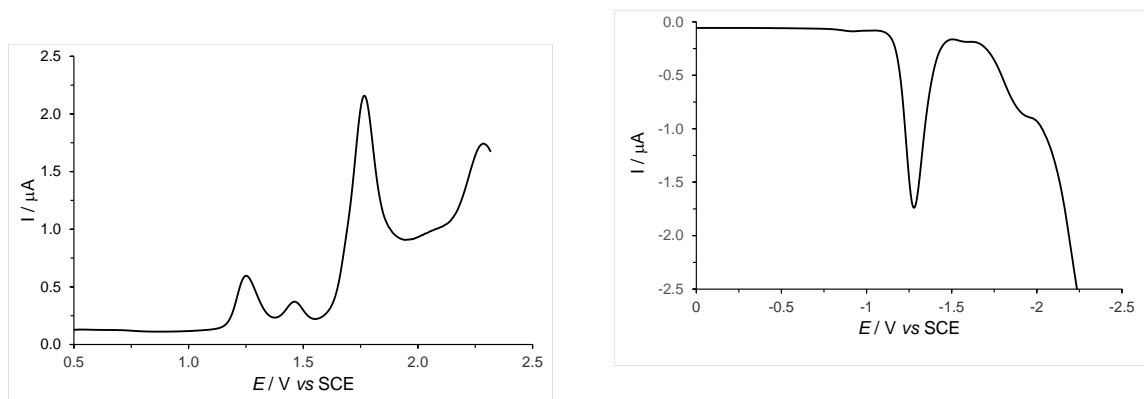


Figure S21. OSWVs: anodic (left) and cathodic (right) scans of complex **1-I**.

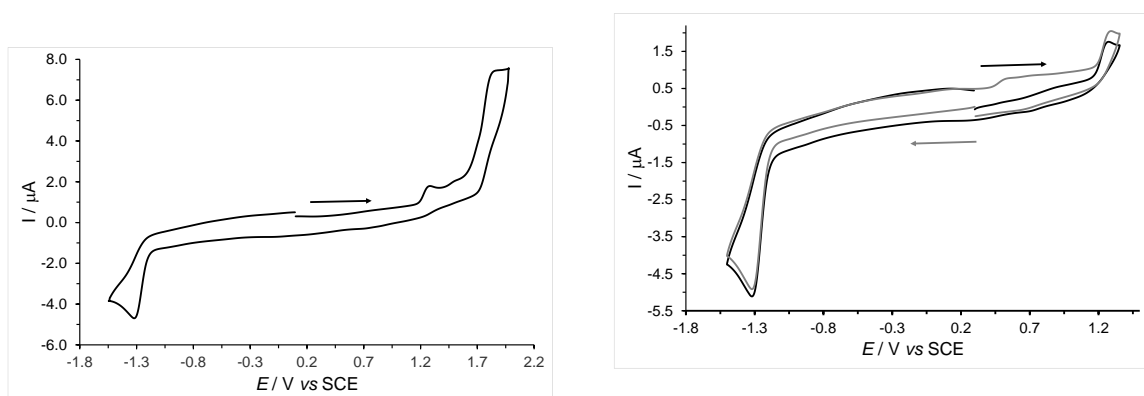


Figure S22. Cyclic voltammograms of complex **1-I** (left), and of its first oxidation and reduction processes (right).

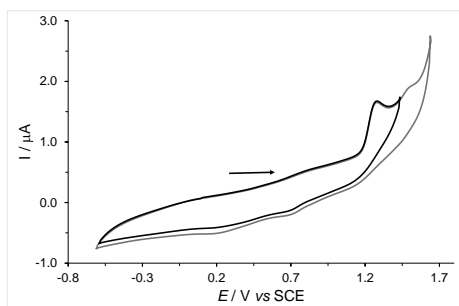


Figure S23. Segmented cyclic voltammograms of complex **1-I** in oxidation at increasing potential.

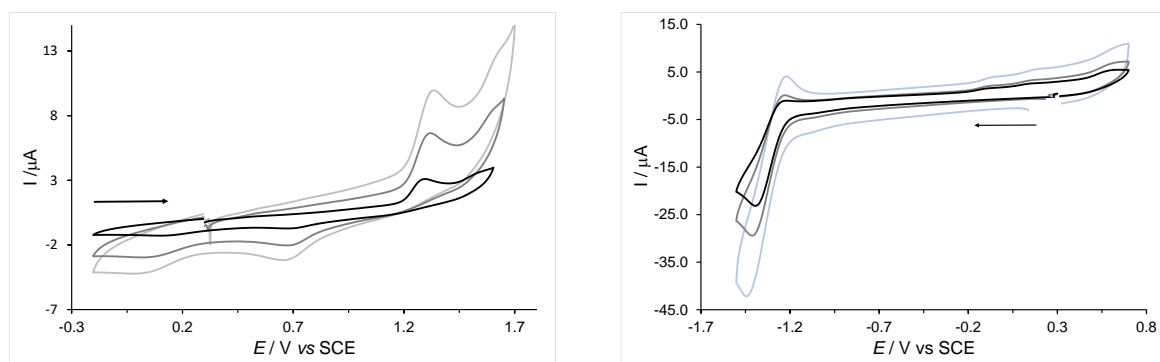


Figure S24. Complex **1-I**: Cyclic voltammograms of the oxidation processes at 1, 5, 10 V/s from bottom-black line to top-grey line (left), and of the first reduction process at 10, 20, 50 V/s from bottom-black line to top-blue line (right).

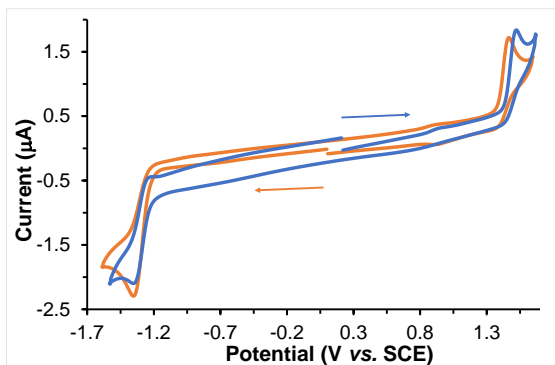


Figure S25. Cyclic voltammograms of the first oxidation and reduction processes of complexes **1-Cl** (blue line) and **1-Br** (orange line) in dichloromethane.

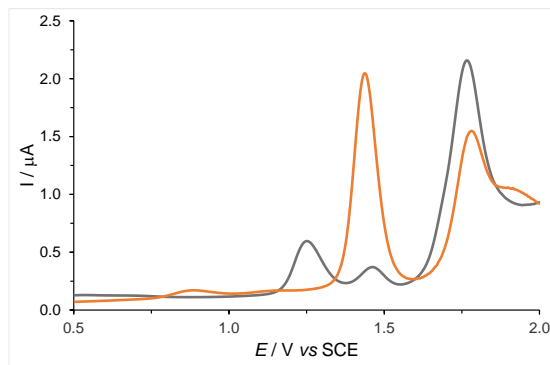


Figure S26. OSWVs: anodic scans of complexes **1-Br** (orange line) and **1-I** (grey line).

Spectroscopy

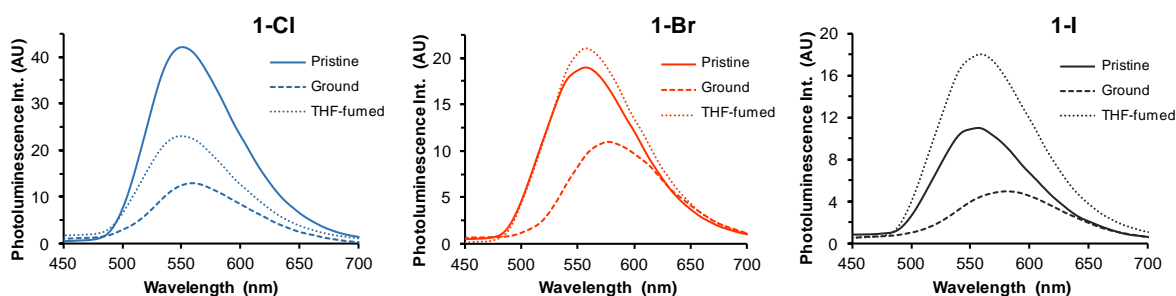


Figure S27. Emission spectra of the three complexes **1-Cl** ($\lambda_{\text{ex}} = 385$ nm), **1-Br** ($\lambda_{\text{ex}} = 388$ nm), and **1-I** ($\lambda_{\text{ex}} = 398$ nm) as microcrystalline pristine powders (solid lines), after grinding (slashed lines), and after fuming the ground powder with THF during 48h (dotted lines). Pristine powder of **1-I** prepared from CH_2Cl_2 solutions. The intensity at the maximum emission wavelength is proportional to the PLQY.

Fluorescence microscopy

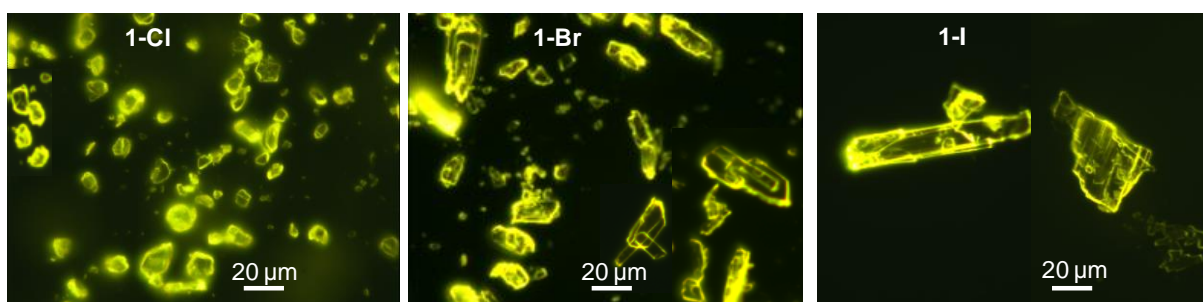


Figure S28. Fluorescence microscopy images of crystals of **1-Cl**, **1-Br** and **1-I** ($\lambda_{\text{ex}} \sim 450\text{--}490$, $\lambda_{\text{em}} > 500$ nm).